An Augmented Lagrangian Method for Autofocused Compressed SAR Imaging

Alper Güngör
Air Platform Radar
Systems Engineering,
ASELSAN Inc., Ankara, Turkey
alpergungor@aselsan.com.tr

Müjdat Çetin
Faculty of Engineering
and Natural Sciences,
Sabancı University, Istanbul, Turkey,
mcetin@sabanciuniv.edu

H. Emre Güven
Advanced Sensing,
ASELSAN Research
ASELSAN Inc., Ankara, Turkey
heguven@aselsan.com.tr

Abstract—We present an autofocus algorithm for Compressed SAR Imaging. The technique estimates and corrects for 1-D phase errors in the phase history domain, based on prior knowledge that the reflectivity field is sparse, as in the case of strong scatterers against a weakly-scattering background. The algorithm relies on the Sparsity Driven Autofocus (SDA) method and Augmented Lagrangian Methods (ALM), particularly Alternating Directions Method of Multipliers (ADMM). In particular, we propose an ADMM-based algorithm that we call Autofocusing Iteratively Re-Weighted Augmented Lagrangian Method (AIRWALM) to solve a constrained formulation of the sparsity driven autofocus problem with an ℓ_p-norm, $p \leq 1$ cost function. We then compare the performance of the proposed algorithm's performance to Phase Gradient Autofocus (PGA) and SDA [2] in terms of autofocusing capability, phase error correction, and computation time.

I. INTRODUCTION

In this paper, we consider the autofocused compressed SAR imaging problem, with 1-D phase errors in the azimuth direction. We model the problem as one of non-convex optimization, and solve it using advanced optimization techniques.

While forming SAR images, it is necessary to correct the errors originating from navigation errors or non-ideal propagation media [1]. Autofocus algorithms are used to estimate and correct these errors, typically following the formation of SAR images. However, in compressive SAR imaging, conventional algorithms do not work well [1]. A Sparsity Driven Autofocus approach [2] has been shown to work well for imaging problems where full data are available within the bandwidth and/or aperture. Nonetheless, it remains a challenge to solve the associated optimization problems in computationally efficient ways for practical use. Our main motivation here is to estimate and correct 1-D phase errors in compressed sensing SAR imaging with high computational efficiency, while forming autofocused SAR images with sparsity priors.

Alternating Direction Method of Multipliers (ADMM) has been successfully applied to signal and image recovery problems [3], [4]. ADMM provides a divide-and-conquer approach by splitting unconstrained multi-objective convex optimization problems, augmenting the Lagrangian with a norm-squared error term, and using a nonlinear block Gauss-Seidel approach on the resultant terms in the optimization problem. The resulting algorithm exhibits guaranteed convergence under mild conditions [3].

We propose a constrained approach based on ℓ_p-norm minimization involving phase errors in the problem set up as

variables as well. The method optimizes over the reflectivities and phase errors jointly, and is based on the Iteratively Re-Weighted Augmented Lagrangian Method (IRWALM) [7], [8] and Sparsity Driven Autofocus (SDA) [2]. For simplicity, we only consider 1-D phase errors, while the method can be extended to other types of phase errors [2], as well. The proposed algorithm is compared to Phase Gradient Autofocus (PGA) and SDA. The results on raw SAR data collected with SARPER™ –airborne SAR system developed by ASELSAN [9]– show the effectiveness of the proposed algorithm. Our primary contribution is the development of a computationally efficient ADMM-based algorithm for sparsity-driven autofocused SAR imaging.

II. BACKGROUND

A. SAR Observation Model

The SAR observation model can be considered linear in relating the image pixels to the data vector. Let us denote the data vector by $\mathbf{y} \in \mathbb{C}^M$, the vector containing image pixels by $\mathbf{x} \in \mathbb{C}^N$, the observation matrix by $\mathbf{B}(\phi) \in \mathbb{C}^{M \times N}$ with $M < N$, and the unknown 1-D phase error term by $\phi \in \Re^n$, where n denotes the number of samples in the azimuth direction. In this paper, we assume that the data vector lies in the phase history domain, and $\mathbf{B}(\phi)$ denotes a 2-D Fourier Transformation with phase correction and consecutive masking. Then, $\mathbf{B}(\phi)$ can be decomposed into three elements as:

$$\mathbf{B}(\phi) = \mathbf{M}\mathbf{P}_\phi\mathbf{U}, \tag{1}$$

where $\mathbf{M} \in \Re^{M \times N}$ is the masking matrix, $\mathbf{P}_\phi \in \mathbb{C}^{N \times N}$ is the diagonal phase error matrix, and $\mathbf{U} \in \mathbb{C}^{N \times N}$ is the 2-D Fourier matrix. Then, the measurement vector $\mathbf{y}$ is given by the model:

$$\mathbf{y} = \mathbf{B}(\phi)\mathbf{x} + \mathbf{n}. \tag{2}$$

$\mathbf{n} \in \mathbb{C}^M$ denotes the additive noise vector, and $\mathbf{P}_\phi$ is the matrix corresponding to multiplication by the phase-error term for each azimuth index i.

While we refer to the corresponding operators using matrix notation, none of the matrices in Eq. (1) are formed explicitly in the implementation. Rather, the transformations are carried out through element-wise multiplications for $\mathbf{M}$ and $\mathbf{P}_\phi$, and FFTs for $\mathbf{U}$.

Algorithm 1: *IRWALM*

1. Set $k = 0$, choose β, $p \leq 1$, $\mu > 0$, $\mathbf{z}_0^{(1)}$, $\mathbf{z}_0^{(2)}$, $\mathbf{d}_0^{(1)}$, $\mathbf{d}_0^{(2)}$
2. **repeat**
3. $\mathbf{r}_k = \mathbf{z}_0^{(1)} + \mathbf{d}_0^{(1)} + \mathbf{B}^H \left(\mathbf{z}_0^{(2)} + \mathbf{d}_0^{(2)} \right)$
4. $\mathbf{x}_{k+1} = \left(\mathbf{I} + \mathbf{B}^H \mathbf{B} \right)^{-1} \mathbf{r}_k$
5. $\mathbf{w}_{k+1} = (\mathbf{x} + \beta)^{(1-p)}$
6. $\mathbf{z}_{k+1}^{(1)} = \frac{1}{\mathbf{w}} \, \text{soft}(\mathbf{w} \times (\mathbf{x}_{k+1} - \mathbf{d}_k^{(1)}), p/\mu)$
7. $\mathbf{z}_{k+1}^{(2)} = \boldsymbol{\Psi}_{\iota_{E(\epsilon, \mathbf{I}, \mathbf{y})}} \left(\mathbf{B}\mathbf{x}_{k+1} - \mathbf{d}_k^{(2)} \right)$
8. $\mathbf{d}_{k+1}^{(1)} = \mathbf{d}_k^{(1)} - \mathbf{x}_{k+1} + \mathbf{z}_{k+1}^{(1)}$
9. $\mathbf{d}_{k+1}^{(2)} = \mathbf{d}_k^{(2)} - \mathbf{B}\mathbf{x}_{k+1} + \mathbf{z}_{k+1}^{(2)}$
10. $k \leftarrow k + 1$
11. **until** some stopping criterion is satisfied.

B. IRWALM

In the context of compressive sensing SAR, where the reflectivity field can be assumed sparse [5], the image formation problem without taking any phase errors into account can be cast as:

$$\underset{\mathbf{x}}{\text{minimize}} \quad \|\mathbf{B}\mathbf{x} - \mathbf{y}\|_2^2 + \lambda \|\mathbf{x}\|_p \; . \tag{3}$$

with $p = 1$, where $\mathbf{B} = \mathbf{M}\mathbf{U}$. Other choices with $p < 1$ yield encouraging results in terms of sparsity enhancement [5]. An alternative form of (3) is the constrained problem:

$$\begin{aligned} \underset{\mathbf{x}}{\text{minimize}} \quad & \|\mathbf{x}\|_p^p \\ \text{subject to} \quad & \|\mathbf{B}\mathbf{x} - \mathbf{y}\|_2 \leq \epsilon \end{aligned} \; . \tag{4}$$

Iterative re-weighting has been used in the solution of optimization problems with non-convex objective functions comprising of p-norms [6]. The IRWALM algorithm [7] takes advantage of the computational efficiency and the robustness of ADMM [4], and provides a method to solve the optimization problem (4). It does so by plugging the approximation of Proximal Mapping Function Ψ of the ℓ_p-norm, which involves iteratively re-weighting the output of the soft thresholding function [7], [8]. IRWALM is given in Algorithm 1.

Computationally efficient techniques to solve the inverse problem in step 4 of IRWALM have been previously proposed in the context of Augmented Lagrangian Methods (ALMs) [3]. β is a small regularization term added in step 5 of IRWALM to avoid numerically unstable divisions. Ψ in step 7 of IRWALM is the Moreau proximal mapping function for the indicator function $\iota_{E(\epsilon, \mathbf{I}, \mathbf{y})}(s)$ corresponding to the data fidelity constraint and given below:

$$\iota_S(\mathbf{s}) = \begin{cases} 0, & \text{if } \mathbf{s} \in S \\ +\infty, & \text{if } \mathbf{s} \notin S \end{cases}, \tag{5}$$

where $E(\epsilon, \mathbf{I}, \mathbf{y})$ is the hypersphere defined by:

$$E(\epsilon, \mathbf{I}, \mathbf{y}) = \left\{ \mathbf{x} \in \mathbb{C}^N : \|\mathbf{B}\mathbf{x} - \mathbf{y}\|_2 \leq \epsilon \right\}. \tag{6}$$

Then, $\boldsymbol{\Psi}$ is given by:

$$\boldsymbol{\Psi}_{\iota_{E(\epsilon,\mathbf{I},\mathbf{y})}}(\mathbf{s}) = \begin{cases} \mathbf{s}, & \text{if } \|\mathbf{s} - \mathbf{y}\|_2 \leq \epsilon \\ \mathbf{y} + \epsilon \frac{(\mathbf{s} - \mathbf{y})}{\|\mathbf{s} - \mathbf{y}\|_2}, & \text{if } \|\mathbf{s} - \mathbf{y}\|_2 > \epsilon \end{cases} \; . \tag{7}$$

C. Sparsity Driven Autofocus (SDA)

The problem of 1-D autofocusing has to do with the estimation of the phase error vector ϕ defined in Section II.A. Sparsity-driven approaches to the autofocus problem in the

---

Algorithm 2: *SDA* [2]

1. Initialize $k = 0$, $\hat{\mathbf{f}}^{(0)} = \mathbf{B}^H y$ and $\mathbf{B}(\hat{\phi}^{(0)}) = \mathbf{B}$
2. **repeat**
3. $\hat{\mathbf{f}}^{(k+1)} = \arg \min_f J(f, \hat{\phi}^{(k)})$
4. $\hat{\phi}^{(k+1)} = \arg \min_\phi J(\hat{\mathbf{f}}^{(k+1)}, \phi)$
5. Update $\mathbf{B}(\hat{\phi}^{(k+1)})$ using $\hat{\phi}^{(k+1)}$ and $\mathbf{B}$
6. Let $k = k + 1$
7. **until** $\|\hat{\mathbf{f}}^{(k+1)} - \hat{\mathbf{f}}^{(k)}\|_2^2 \, / \, \|\hat{\mathbf{f}}^{(k+1)}\|_2^2$ is less than a predetermined threshold

---

literature have provided encouraging results [2], [10], [11]. Sparsity-Driven Autofocus (SDA) algorithm corrects phase errors and enhances the resolution of SAR images by exploiting the sparsity in the image domain [2]. The algorithm addresses problems with phase errors that are (i) one-dimensional, (ii) 2-D separable, (iii) 2-D non-separable. The phase-error dependence is denoted with ϕ in the formulation [2]:

$$\arg \min_{\mathbf{x}} \|\mathbf{y} - \mathbf{B}(\phi)\mathbf{x}\|_2^2 + \lambda \|\mathbf{x}\|_1 \tag{8}$$

In this paper, we only consider 1-D phase errors in azimuth direction. The algorithm divides the problem to two, and solves two sub-problems separately in an alternating fashion, iteratively. Let us define the function $J(f, \phi)$ as:

$$J(f, \phi) = \|\mathbf{y} - \mathbf{B}(\phi)\mathbf{f}\|_2^2 + \lambda \|\mathbf{f}\|_1 \tag{9}$$

Then, at each step, SDA minimizes each variable consecutively, and updates the observation matrix. The SDA approach is given in Algorithm 2, where step 5 performs the updates:

$$\hat{\phi}_{1-D}^{(k+1)}[m] = -\arctan \left(\frac{Im \left\{ \hat{\mathbf{f}}^{(k+1)H} \bar{\mathbf{B}}_m(\phi^{(k)})^H \bar{\mathbf{g}}_m \right\}}{Re \left\{ \hat{\mathbf{f}}^{(k+1)H} \bar{\mathbf{B}}_m(\phi^{(k)})^H \bar{\mathbf{g}}_m \right\}} \right), \tag{10}$$

$$\bar{\mathbf{B}}_m \left(\hat{\phi}_{1-D}^{(k+1)}[m] \right) = \exp \left(j\hat{\phi}_{1-D}^{(k+1)}[m] \right) \bar{\mathbf{B}}_m(\phi^{(k)}), \tag{11}$$

where $\bar{\mathbf{B}}_m$ and $\bar{\mathbf{g}}_m$ denote the rows with indices $m + kn$ of $\bar{\mathbf{B}}_m$ and $\bar{\mathbf{g}}_m$, respectively and Eq. (11) performs the update:

$$\mathbf{P}_{\phi^{(k+1)}}[i, i] = \mathbf{P}_{\phi^{(k)}}[i, i] \cdot \exp \left(j\phi^{(k+1)}[i \bmod n] \right),$$
$$\text{for all } i. \tag{12}$$

in order to iteratively estimate the phase error ϕ.

III. AN AUTOFOCUSED COMPRESSED SAR IMAGING METHOD

A. AIRWALM

The SDA algorithm solves sub-problems regarding the minimization of the regularized data fidelity error and the estimation of the phase error separately, in an alternating fashion within an iterative framework. A different approach to the problem at hand is to solve the following problem, instead of solving the unconstrained problem in step 3 of SDA:

$$\begin{aligned} \underset{\mathbf{x}, \phi}{\text{minimize}} \quad & \|\mathbf{x}\|_1 \\ \text{subject to} \quad & \|\mathbf{B}(\phi)\mathbf{x} - \mathbf{y}\|_2 \leq \epsilon \end{aligned} \tag{13}$$

For SAR imaging problems, it is somewhat easier to select ϵ, the data fidelity error bound in Eq. (13), than choosing λ,

the regularization parameter in Eq. (8). Moreover, the change of the minimization problem at step 3 of SDA, does not affect the solution at step 4, since one can select λ such that both algorithms reach a solution with the same 1-norm and data fidelity error in the unconstrained form as the constrained formulation with a corresponding ϵ value. Therefore, we assume that the constrained algorithm chooses such a λ to set the error bound to ϵ. This justifies that step 4 of SDA has equivalent solutions in constrained and unconstrained forms.

We take our approach one step further and instead of (13), we solve:

$$
\begin{aligned}
\underset{\mathbf{x},\phi}{\text{minimize}} \qquad & \|\mathbf{x}\|_p^p \\
\text{subject to} \qquad & \|\mathbf{B}(\phi)\mathbf{x} - \mathbf{y}\|_2 \le \epsilon
\end{aligned}
\tag{14}
$$

Since the use of p-norms further enhances sparsity, this change is expected to result in a more accurate estimation for the phase error.

Also, since the modification involves the regularization term in the unconstrained form, and does not depend on ϕ, step 4 of SDA remains the same. We only change the sub-problem in step 3 of SDA, and use a variation of ADMM, IRWALM for the solution and reach a computationally efficient algorithm. The stopping criterion for the inner loop can be chosen as "**until** $k = 1$" in order to stop the inner loop immediately after running once. Even then, the algorithm provides an estimate of the phase error. To reach a more accurate result, instead of running the inner loop only once, we place the phase estimation step inside IRWALM, keeping vectors $\mathbf{z}_k, \mathbf{d}_k$ and $\mathbf{x}_k$ intact. We run the algorithm with the initial setting:

$$
\mathbf{z}_0^{(1)} = \mathbf{z}_1^{(1)}, \mathbf{z}_0^{(2)} = \mathbf{z}_1^{(2)}, \tag{15}
$$

$$
\mathbf{v}_0^{(1)} = \mathbf{v}_1^{(1)}, \mathbf{v}_0^{(2)} = \mathbf{v}_1^{(2)}, \tag{16}
$$

$$
\mathbf{x}_0 = \mathbf{x}_1. \tag{17}
$$

This results in faster convergence, as well as a more accurate phase error estimation. The resulting approach, Autofocusing Iteratively Re-Weighted Augmented Lagrangian Method (AIRWALM), is presented in Algorithm 3.

Algorithm 3: *Autofocusing Iteratively Re-Weighted Augmented Lagrangian Method (AIRWALM)*

---
1. Set $\mathbf{B}(\hat{\phi}^{(0)}) = \mathbf{B}$, $k = 0$, $\hat{\mathbf{x}}^{(0)} = \mathbf{B}(\phi^{(0)})^H y$
choose $\mu > 0$, $\mathbf{z}_0^{(1)}, \mathbf{z}_0^{(2)}, \mathbf{d}_0^{(1)}, \mathbf{d}_0^{(2)}, 0 < p < 1$
2. **repeat**
3. $\mathbf{r}_k = \mathbf{z}_k^{(1)} + \mathbf{d}_k^{(1)} + \mathbf{B}(\phi^{(k)})^H \left(\mathbf{z}_k^{(2)} + \mathbf{d}_k^{(2)} \right)$
4. $\mathbf{x}_{k+1} = \left(\mathbf{I} + \mathbf{B}(\phi^{(k)})^H \mathbf{B}(\phi^{(k)}) \right)^{-1} \mathbf{r}_k$
5. $\mathbf{w}_{k+1} = (\mathbf{x} + \beta)^{(1-p)}$
6. $\mathbf{z}_{k+1}^{(1)} = \frac{1}{\mathbf{w}} \text{soft}(\mathbf{w} \times (\mathbf{x}_{k+1} - \mathbf{d}_k^{(1)}), p/\mu)$
7. $\mathbf{z}_{k+1}^{(2)} = \mathbf{\Psi}_{\iota_{E(\epsilon,\mathbf{I},\mathbf{y})}} \left(\mathbf{B}(\phi^{(k)})\mathbf{x}_{k+1} - \mathbf{d}_k^{(2)} \right)$
8. $\mathbf{d}_{k+1}^{(1)} = \mathbf{d}_k^{(1)} - \mathbf{x}_{k+1} + \mathbf{z}_{k+1}^{(1)}$
9. $\mathbf{d}_{k+1}^{(2)} = \mathbf{d}_k^{(2)} - \mathbf{B}(\phi^{(k)})\mathbf{x}_{k+1} + \mathbf{z}_{k+1}^{(2)}$
10. $\hat{\phi}_{1-D}^{(k+1)}(m) = -\arctan\left(\frac{Im\left\{ \hat{\mathbf{x}}^{(k+1)H} \bar{\mathbf{B}}_m(\phi^{(k)})^H \bar{\mathbf{y}}_m \right\}}{Re\left\{ \hat{\mathbf{x}}^{(k+1)H} \bar{\mathbf{B}}_m(\phi^{(k)})^H \bar{\mathbf{y}}_m \right\}} \right)$
11. $\bar{\mathbf{B}}_m \left(\hat{\phi}_{1-D}^{(k+1)}(m) \right) = \exp\left(j\hat{\phi}_{1-D}^{(k+1)}(m) \right) \bar{\mathbf{B}}_m(\phi^{(k)})$
12. $k \leftarrow k + 1$
13. **until** some stopping criterion is satisfied.

From an ADMM point of view, we update the observation matrix at the end of each iteration. Although the known

guarantees for convergence of ADMM are not valid in this case, in practice we have observed a consistent behavior of the algorithm with non-convex functions.

The algorithm requires 2 FFTs per iteration, which can be calculated at the cost of $O(N \log(N))$. All other operations are element-wise operations and have a cost of $O(N)$.

IV. RESULTS

We implemented the proposed algorithm in MATLAB. The experiments were conducted on a workstation with Intel Core i5-3470 CPU and 8 GB of RAM. All values are initialized to zero except for $\mathbf{z}_0^{(2)}$, which is initialized to $\mathbf{y}$. μ is chosen as 300 for AIRWALM.

First, we experimented on the Slicy data, which are from a public SAR data set, provided by U.S Air Force Research Laboratory (AFRL) [12]. The scene reconstructed using the conventional polar format algorithm from full-aperture, full-bandwidth data without phase errors is shown in Fig. 1.a. For our experiments, we consider a scenario in which only 39% of that data, sampled through a random mask shown in Fig. 1.b, are available. Other, more structured sampling schemes can of course be considered as well. We also add an artificial phase error to compressively sensed data. The images obtained by conventional imaging and after the application of the PGA algorithm are shown in Fig. 1.c and 1.d, respectively. Although PGA achieves some degree of focusing, it cannot provide accurate localization of all scatterers in this limited-data scenario.

For Algorithm 3, the stopping criterion for the algorithm is chosen as "**until** $k = 300$". Figures 1.e–f show the resulting images for AIRWALM for $p = 0.3$ and $p = 1.0$. The proposed approach results in better and more accurate localization of all dominant scatterers. However, we also observed that the phase error estimation step impacts the image reconstruction performance significantly. The phase error estimation error is shown in Fig 2. While a constant offset in the phase error estimate has no impact on the magnitudes of the image pixels, a linear offset causes a circular shifting of the image. Since the sparsity of the image does not change in either case, the model we currently present is indifferent to constant and linear phase errors, which can be safely ignored from an imaging point of view [13].

As shown in Fig. 2, PGA can not correctly estimate the phase error while AIRWALM reaches a nearly constant offset, with little effect on the magnitude image. To quantify the phase error estimation performance, we fit a line to each of these results with minimum square error, then check the Root Mean Square (RMS) value of fitting error. The RMS values for different values of p and RMS value for PGA can be found in Table I. To analyze the convergence speed versus the value of parameter p, the RMS values at each iteration are plotted in Fig. 3. One can observe from Fig. 3 that smaller p allows quicker convergence with slightly greater RMS error on average.

To further analyse the performance of the proposed method, we validated our approach using the raw data collected using SARPER™ [9] –airborne SAR system developed by ASELSAN. The reference image with full-aperture data which
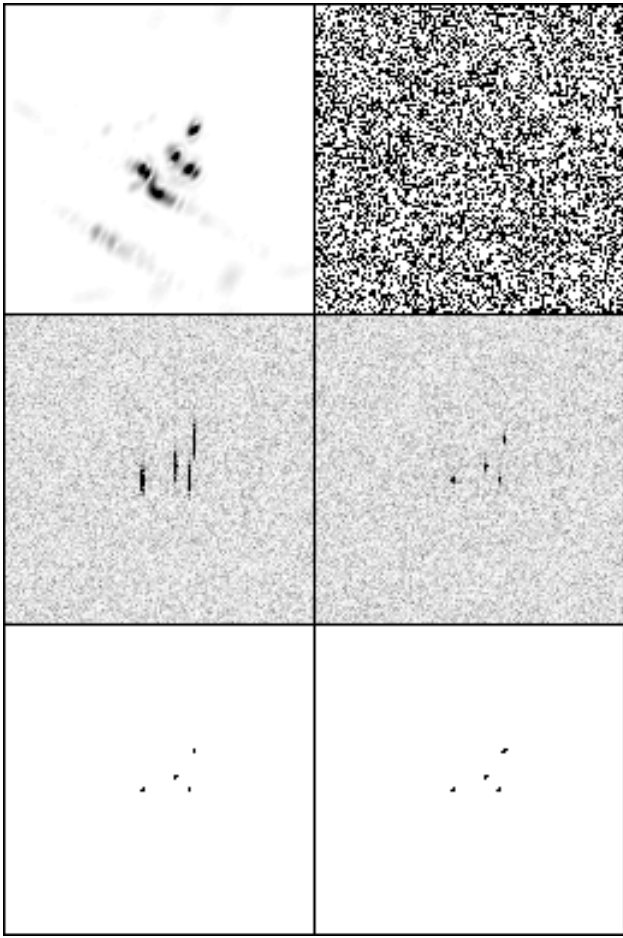
Fig. 1. a. Reference slicy image (upper-left), b. Available samples in 2-D Fourier space (39% of all points) (upper-right), c. Conventionally reconstructed image (middle-left), d. Conventionally reconstructed image after using PGA (middle-right), e. Image reconstructed with AIRWALM $\ell_{0.3}$ (lower-left), f. Image reconstructed with AIRWALM ℓ_1 (lower-right)

includes phase errors is shown in Fig 4.a. For our experiments, we again consider a limited-data scenario. The available samples in the 2-D Fourier space are shown in Fig 4.b. The conventional reconstruction, and the reconstructed image with PGA are shown in Figs. 4.c–d, respectively. The image reconstruction performances of PGA and conventional imaging do not appear to be satisfactory. Figs. 4.e–f show the reconstructions with the proposed AIRWALM with $p = 0.3$ and $p = 1$, respectively, after 600 iterations. The phase error estimates are shown in Fig. 5. Since a ground-truth is not available for the phase error, we draw comparisons to the result of PGA run with full data, as a reference. In this limited-data scenario, we observe that the phase error estimates produced by AIRWALM are better than those of PGA, in terms of their similarity to the reference phase error estimates obtained by PGA from full data.

Dataset	$\ell_{0.3}$	$\ell_{0.5}$	$\ell_{0.8}$	ℓ_1	PGA
Slicy	0.0281	0.0272	0.0263	0.0258 s	0.1233

TABLE I.   RMS VALUES (RADIANS) FOR PGA AND AIRWALM FOR SLICY DATA (128x128) WHERE 39% OF THE DATA ARE ASSUMED TO BE AVAILABLE
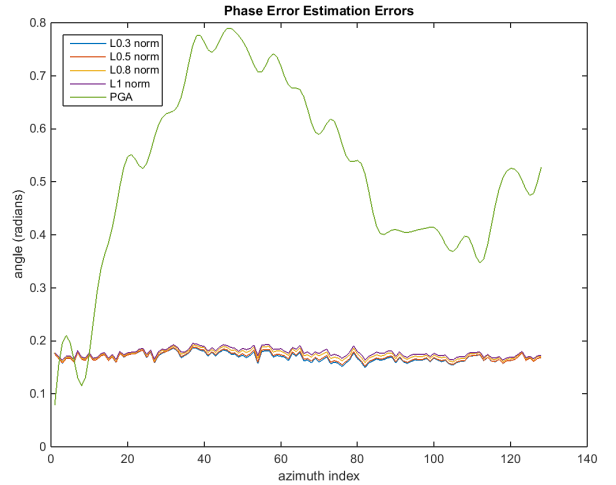

Fig. 2.   Phase error estimation errors of AIRWALM and PGA.
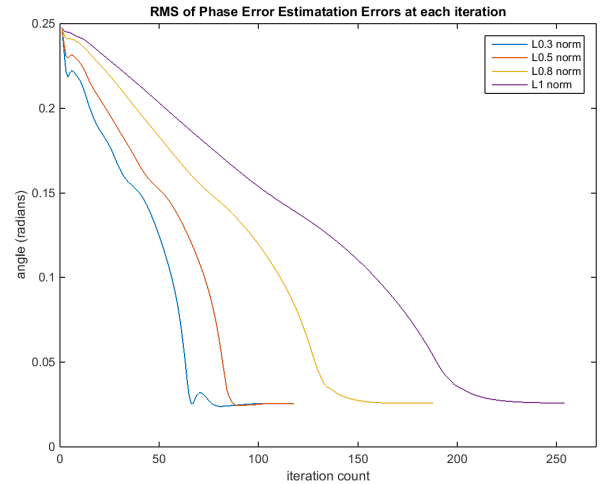

Fig. 3.   RMS value of phase error estimation errors versus iteration count of AIRWALM.

The comparison of AIRWALM to SDA regarding computational performance is given in Table II. Both algorithms are run without reduction in data. As it can be seen from the table, AIRWALM results in a faster solution in each of the studied cases.

Dataset	$\ell_{0.3}$	$\ell_{0.5}$	$\ell_{0.8}$	ℓ_1	SDA
Slicy	0.74 s	0.89 s	1.24 s	1.05 s	1.47 s
SARPER™	1.47 s	1.63 s	2.01 s	1.70 s	3.45 s

TABLE II.   COMPUTATION TIMES (SECONDS) FOR SDA AND AIRWALM FOR SLICY DATA (128x128) AND RAW SARPER™ DATA (128x128), WHERE FULL DATA ARE ASSUMED TO BE AVAILABLE

V.   DISCUSSION

In this paper, we presented a computationally efficient method based on ADMM for the problem of autofocused
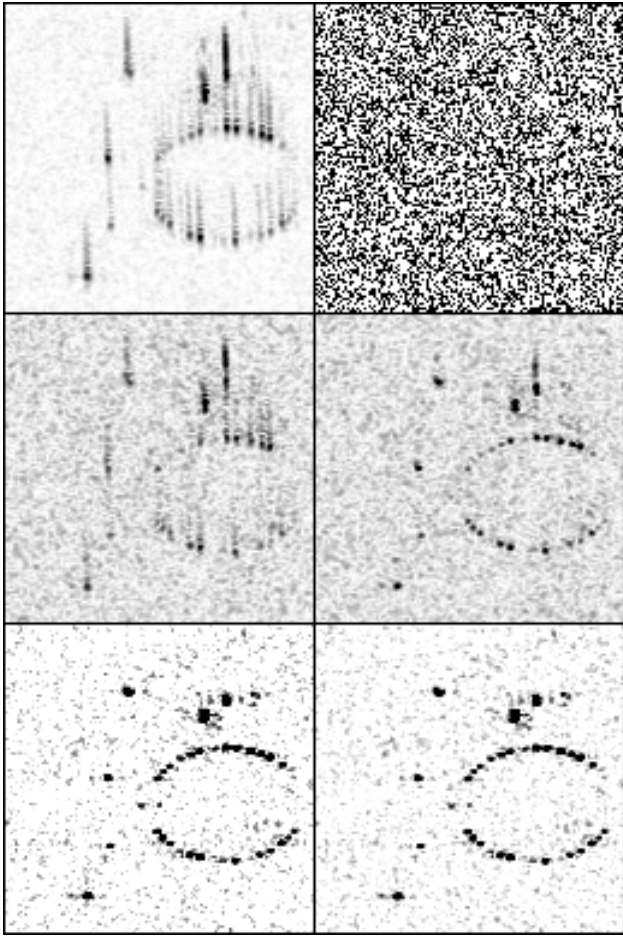
Fig. 4.   a. Image reconstruction from full-bandwidth / full-aperture data (upper-left), b. Available samples in 2-D Fourier space (39% of all points) (upper-right), c. Conventionally reconstructed image (middle-left), d. Conventionally reconstructed image after using PGA (middle-right), e. Image reconstructed with AIRWALM $\ell_{0.3}$ (lower-left), f. Image reconstructed with AIRWALM ℓ_1 (lower-right).
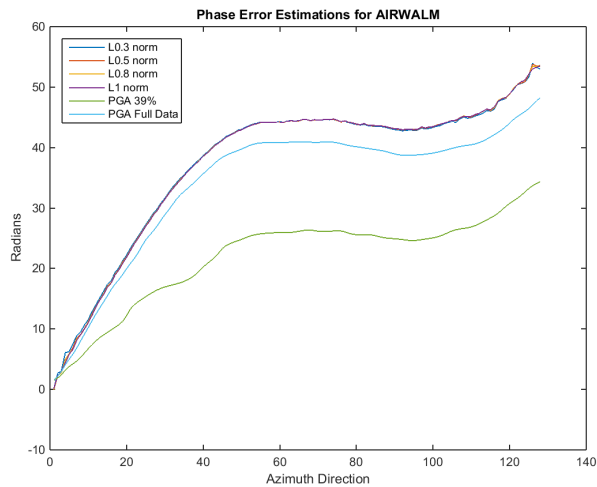

Fig. 5.   Phase error estimations by AIRWALM and PGA with 39% and PGA with full data.

compressed SAR imaging. The proposed method (AIRWALM) exhibits better autofocusing capability, improved contrast, and more accurate estimation of the phase errors, especially in limited data scenarios, as compared to the well-known PGA approach. As compared to SDA, the proposed approach offers reduced computation time and a slightly easier choice of the hyperparameter involved in the problem.

While what we propose here is a joint imaging and phase error estimation approach, one could also use our approach just for accurate estimation of phase errors. In particular, given the forward model updated with phase errors estimated by our method, one could then use any image formation approach exploiting the phase error correction achieved by our method.

REFERENCES

[1] N. Kelly, M. Yaghoobi, M. Davies: *Sparsity-Based Autofocus for Undersampled Synthetic Aperture Radar*, IEEE Trans. Aerospace and Electronics Systems, vol. 50, no. 2, pp. 972–986, April 2014.

[2] N. O. Onhon, M. Cetin: *A Sparsity-Driven Approach for Joint SAR Imaging and Phase Error Correction*, IEEE Trans. Image Processing, vol. 21, no. 4, pp. 2075–2088, April 2012.

[3] M. Afonso, J. M. Bioucas-Dias, M. A. T. Figueiredo: *An Augmented Lagrangian approach to the constrained optimization formulation of imaging inverse problems*, IEEE Trans. Image Processing, vol. 20, no. 3, pp. 681–695, March 2011.

[4] S. Boyd, N. Parikh, E. Chu, B. Peleato, and J. Eckstein, "Distributed optimization and statistical learning via the alternating direction method of multipliers," *Foundations and Trends in Machine Learning*, vol. 3, no. 1, pp. 1–122, 2011.

[5] M. Cetin, W. C. Karl: *Feature-enhanced synthetic aperture radar image formation based on nonquadratic regularization*, IEEE Trans. Image Processing, vol. 10, no. 4, pp. 623–631, April 2001.

[6] R. Chartrand and W. Yin, "Iteratively reweighted algorithms for compressive sensing," in *International Conference on Acoustics, Speech, and Signal Processing*. IEEE, 2008.

[7] H. E. Guven and M. Cetin, "An augmented Lagrangian method for sparse sar imaging," in *10th European Conference on Synthetic Aperture Radar (EUSAR 2014)*. EU, 2014.

[8] H. E. Guven, A. Gungor and M. Cetin, "An augmented Lagrangian method for image reconstruction with multiple features," submitted to *International Conference on Image Processing (ICIP 2015)*, September 2015.

[9] ASELSAN website for SARPER™: http://www.aselsan.com.tr/en-us/capabilities/radar-systems/

[10] S. Ugur, O. Arikan, A. C. Gurbuz: *SAR image reconstruction by expectation maximization based matching pursuit*, Digital Signal Processing, vol. 37, pp. 75–84, February 2015.

[11] Ender, Joachim H. G, "Autofocusing ISAR images via sparse representation," in *9th European Conference on Synthetic Aperture Radar (EUSAR 2012)*. EU, 2012.

[12] Air Force Research Laboratory, Model Based Vision Laboratory, Sensor Data Management System MSTAR Web Page: www.mbvlab.wpafb.af.mil/public/sdms /datasets/mstar.

[13] C. Jakowatz, D. Wahl, P. Eichel, D. Ghiglia, and P. Thompson, *Spotlight-Mode Synthetic Aperture Radar: A Signal Processing Approach,* (4th ed.) Dordrecht, The Netherlands: Kluwer Academic Publishers, 1999.